Quantized Periodic Orbits in Large Antidot Arrays

D. Weiss,[1] K. Richter,[1],[a] A. Menschig,[2] R. Bergmann,[2] H. Schweizer,[2] K. von Klitzing,[1] and G. Weimann[3]

[1] *Max-Planck-Institut für Festkörperforschung, D-7000 Stuttgart 80, Germany*

[2] *IV Physikalisches Institut der Universität Stuttgart, D-7000 Stuttgart 80, Germany*

[3] *Walter-Schottky Institut der Technischen Universität München, D-8046 Garching, Germany*

(Received 12 March 1993)

The resistivity ρ_{xx} measured in large antidot arrays as a function of an applied perpendicular magnetic field B displays distinct quantum oscillations at very low temperatures. These oscillations characteristically differ from conventional Shubnikov–de Haas oscillations which are periodic in $1/B$. A crossover to B periodic oscillations at low B discloses the influence of the imposed potential. Applying semiclassical *periodic orbit theory* to the nonintegrable (chaotic) electron motion in the antidot lattice we attribute these phenomena to the quantization of few fundamental periodic orbits.

PACS numbers: 73.20.Dx, 03.65.Sq, 05.45.+b, 73.50.Jt

Magnetoresistance oscillations in *mesoscopic* conductors, periodic in B, are usually considered a manifestation of the Aharanov-Bohm (AB) effect [1]. A magnetic flux $\Phi = B\mathcal{A}$ threaded through a loop smaller than the phase coherence length ℓ_Φ alters the phase of the electrons passing along either side, so that the resistance is modulated by the interference of the phase-shifted wave functions. The oscillations are periodic in $(h/e)\mathcal{A}^{-1}$ and reflect the successive addition of one flux quantum h/e through the loop area $\mathcal{A}$. To observe $(h/e)\mathcal{A}^{-1}$ periodic oscillations in multiple connected rings [2] the electron wave function needs to be coherent across the *entire* array. Antidot superlattices [3] consisting of a periodic array of holes "drilled" through a two-dimensional electron gas (2DEG) are closely related to such a large, multiply connected ring geometry. In the past, B periodic features in the resistivity of lateral superlattices [4–6] have been ascribed to the AB effect [4,6]. In this Letter we show that B periodic oscillations which we observe in antidot arrays with dimensions large compared to ℓ_Φ result from a modified electron energy spectrum. We find that the spectrum is dominated by few *quantized* periodic orbits. In contrast to the AB effect this latter mechanism requires phase coherence only on a length scale given by the circumference of the cyclotron orbit *but not* across the entire lattice.

We fabricate antidot arrays from high-mobility GaAs-AlGaAs heterojunctions which, at 4.2 K, have carrier densities $n_s \sim (1.4\text{–}2.8)\times 10^{11}\,\mathrm{cm}^{-2}$ and mobilities $\mu \sim (0.5\text{–}1.2)\times 10^6\,\mathrm{cm}^2/\mathrm{V\,s}$. A periodic (square) array of holes with period $a = 200$ nm or 300 nm is defined by electron beam lithography on top of a 100 μm wide Hall bar [Fig. 1(a), inset] and transferred into the 2DEG by dry etching [7]. These antidots, forming impenetrable barriers for the electrons, are characterized by their (normalized) cross section $\hat{d} = d/a$ and the steepness of the imposed repulsive potential which depends on the lithographic diameter, and the depletion region around the holes. The electron mean free path in our devices, $\ell_e = m^* v_F \mu/e$, is 3 to 10 μm and is comparable to the phase coherence length ℓ_ϕ [8]. Here, m^* is the electron effective mass, and v_F the Fermi velocity. Although $\ell_e, \ell_\Phi >> a$, the antidot array is *macroscopic*; its dimensions are large compared to ℓ_Φ and ℓ_e.

Recent experiments in antidot arrays unveiled a series of low B resistance peaks at *commensurate* B, for which the classical cyclotron orbit with radius $R_c = \hbar(2\pi n_s)^{1/2}/eB$ encompasses a particular number of antidots [5,9]. While the basic mechanisms can be understood in a simple circular orbit analysis [5] a detailed description of the transport anomalies involves the peculiar electron dynamics in an antidot potential landscape: the ρ_{xx} anomalies stem from electrons trapped on *classically chaotic* trajectories for commensurate B [10].

Here, we explore transport anomalies in a temperature regime where the *quantization* of nonintegrable electron motion comes into play. Measurements of ρ_{xx} at $T \sim 0.4$ K display quantum oscillations superimposed upon the low B resistance anomalies. Corresponding data for a sample with large $\hat{d} \sim 0.5$ [11] are shown in Fig. 1(a) where we compare ρ_{xx} from both patterned and unpatterned sample segments. In the unpatterned part, $1/B$ periodic Shubnikov–de Haas (SdH) oscillations reflect the Landau energy spectrum. The quantum oscillations in the antidot segment reveal quite different behavior [12]. The oscillations are *periodic in* B with period $\Delta B \sim 0.105\ \mathrm{T} \sim h/ea^2$ corresponding to the addition of approximately one flux quantum through the antidot unit cell [Fig. 1(b)]. At 4.7 K, the quantum oscillations are smeared out while the characteristic ρ_{xx} peak at $2R_c = a$, attributed to trapped electrons whirling around one antidot, persists. The oscillations periodic in B dominate only the low B regime ($2R_c > a - d$); at high B, the sample behaves as if unpatterned, and ρ_{xx} displays minima which are $1/B$ periodic reflecting quantization of essentially *unperturbed* cyclotron orbits [Fig. 1(a), left inset]. In Fig. 1(c) we plot the oscillation index η for both the high and low field regimes versus inverse magnetic field

0031-9007/93/70(26)/4118(4)$06.00

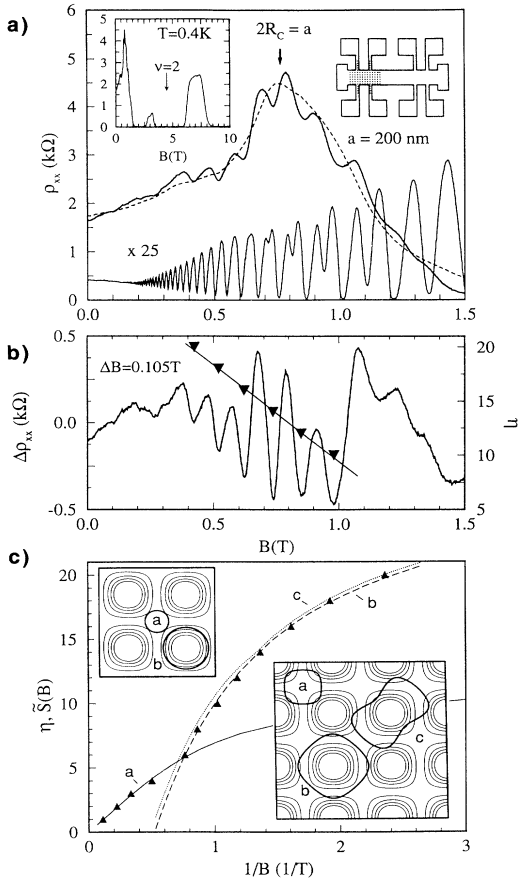

FIG. 1. (a) ρ_{xx} measured in patterned (top traces) and unpatterned (bottom trace) segments of the same sample for $T = 0.4$ K (solid lines) and 4.7 K (dashed line). Left inset: ρ_{xx} up to 10 T; filling factor $\nu = 2$ is marked. Right inset: Sample layout. (b) $\rho_{xx}(T = 0.4\ \text{K}) - \rho_{xx}(T = 4.7\ \text{K})$ vs B. For $B < 1$ T the ρ_{xx} minima positions (triangles) are spaced by $\Delta B = 105$ mT. (c) Triangles mark $1/B$ positions of ρ_{xx} minima. Solid, dashed, and dotted lines are calculated reduced actions $\tilde{S}(1/B)$ of orbits (a), (b), and (c), respectively. These orbits are shown for $1/B = 0.6\ \text{T}^{-1}$ (top) and $1/B = 2.7\ \text{T}^{-1}$ (bottom inset).

positions of the ρ_{xx} minima. At high B, η is the filling factor $\nu = n_s h/eB$ counting the number of occupied (spin-split) Landau levels. At low B the antidot potential strongly mixes different Landau levels and the filling factor loses its physical meaning.

Deviations from a linear $1/B$ dependence in Fig. 1(c) can be assigned to the periodic orbits shown for an intermediate and low B value in the insets of Fig. 1(c). These orbits play a central role in explaining the positions of the ρ_{xx} extrema. This is evident from the calculated action $\tilde{S}(B)$ of these orbits, displayed in Fig. 1(c). These calculations will be addressed below.

Oscillations periodic in B are *not an inherent* property of antidot arrays. Data taken from a superlattice

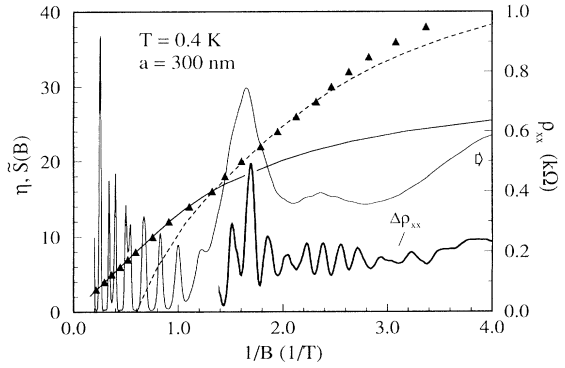

FIG. 2. ρ_{xx} and $\Delta\rho_{xx}$ (arbitrary units) vs $1/B$. The oscillation index η labels ρ_{xx} minima positions on the $1/B$ scale (triangles). Solid line: Calculated action $\tilde{S}(B)$ for an orbit between four antidots. Dashed line: $\tilde{S}(B)$ for electron encompassing one antidot.

with smaller $\hat{d} \sim 0.4$ [11] are shown in Fig. 2. In contrast to the data of Figs. 1(a) and 1(b) the positions of the ρ_{xx} minima are nearly equidistant on the $1/B$ scale but display similar deviations for intermediate B where the low field anomalies begin to disappear (between 0.6 T and 1 T). Again, the experimental data are best described by the action calculated for an orbit between four and around one antidot. The crossover from B periodic, AB-like oscillations to $1/B$ periodic, SdH-type oscillations, controlled by $\hat{d}$, provides further evidence that the AB effect is not the origin of our observations. In the following we assume that, as usual for quantum transport, $\rho_{xx} \sim d^2(E, B)$ probes the electron density of states $d(E, B)$ at the Fermi energy ϵ_F [13]. Hence we focus on the level density below.

Quantum mechanical calculations [14] show a complicated magnetic band structure for antidot arrays which is difficult to interpret. An alternative method to obtain information about $d(E, B)$ is based on the *periodic orbit theory* developed by Gutzwiller [15] and others [16]. Within this framework [17] the oscillatory part of $d(E, B)$ for a (generally) *nonseparable, classically chaotic* system can be obtained by coherent summation over contributions $A \exp[i(S/\hbar + \pi\alpha/2)]$ from *each* periodic orbit of the system [15]. Here $S(E, B) = \oint \mathbf{p}\, d\mathbf{q}$ is the classical action, α the Maslov index, and A depends on the stability of the periodic orbit. While the calculation of *individual* semiclassical energy levels for chaotic systems is still an open problem [17] one can approximate a smoothed $d(E, B)$ using a limited number of (fundamental) periodic orbits [18]. In experiment, scattering and finite temperatures limit the resolution of closely spaced energy levels. Both *stable* and *unstable* periodic orbits contribute to $d(E, B)$. Approximate Einstein-Brillouin-Keller quantization [19] of the motion in the vicinity of an isolated *stable* periodic orbit with action $S(E, B)$ yields δ spikes in $d(E, B)$ (i.e., the Landau ladder for cyclotron orbits

in 2DEG systems) at E, B values satisfying the quantization condition

$$S(E,B) = 2\pi\hbar[n + (k + \tfrac{1}{2})\gamma(E,B) + \tfrac{1}{4}\alpha] \,. \qquad (1)$$

In Eq. (1), n counts the number of nodes of an associated wave function along the stable periodic orbit, and k labels quantized vibrational motion with frequency γ perpendicular to the orbit [19,20]. Here we use $k = 0$. *Unstable* periodic orbits give rise to modulations in $d(E,B)$, usually not related to individual quantum states [16]. For those, $\gamma \equiv 0$ holds, and Eq. (1) describes maxima in the $d(E,B)$ modulation. Equation (1) implies that adjacent maxima are spaced by $\Delta B = B_n - B_{n-1} \approx 2\pi\hbar/(\partial S/\partial B)$. Generally, $\partial S/\partial B$ is large for long periodic orbits causing high frequency oscillations (small ΔB), not resolved experimentally. In contrast, short (fundamental) periodic orbits result in a low frequency oscillation of $d(E,B)$; it turns out that only a few of these dominate the spectrum [18].

To find the relevant periodic orbits, we first study the electron dynamics in a model antidot array. Following recent work by Fleischmann, Geisel, and Ketzmerick [10] we use the Hamiltonian

$$H = \epsilon_F = \frac{1}{2m^*}(\mathbf{p} - e\mathbf{A})^2 + U_0\left[\sin\left(\frac{\pi x}{a}\right)\sin\left(\frac{\pi y}{a}\right)\right]^{\beta} \qquad (2)$$

and solve the corresponding classical equations of motion at fixed Fermi energy ϵ_F. Here, $\mathbf{A}$ is the vector potential. After normalizing energies and lengths in Eq. (2) by ϵ_F and a, respectively (without changing the notation), we adjust the effective antidot diameter $\hat{d}$ at $\epsilon_F = 1$ by the (now dimensionless) prefactor U_0 while β controls the steepness of the potential.

After integrating the Hamiltonian equations of motion numerically, we search for periodic orbits, and calculate their actions

$$S(B) = \oint (m^*\mathbf{v} + e\mathbf{A})d\mathbf{r} = m^* \oint \mathbf{v}\, d\mathbf{r} - eB\mathcal{A}(B) \,, \qquad (3)$$

and stability indices (Liapunov exponents or winding numbers γ). $B\mathcal{A}(B)$ in Eq. (3) is the enclosed flux through a periodic orbit and $\mathbf{v}$ is the electron velocity. To compare with experiment we calculate the reduced action $\tilde{S}(B)$

$$\tilde{S}(B) \equiv 2\frac{S(B)}{h} - \gamma(B) - \frac{\alpha}{2} - 1 = 2n;\ n = 1, 2, ..., \qquad (4)$$

where $2n$ now labels *minima* in $d(E,B)$. Note that the y axis of Figs. 1(c) and 2 represents $\tilde{S}$, where even η are described by Eq. (4). At high B, $2n$ is the filling factor ν [21]. Calculated traces of $\tilde{S}(B)$ are shown in Figs. 1(c) and 2. Three periodic orbits, displayed in the insets of Fig. 1(c), are sufficient to explain the minima positions of ρ_{xx}. These are (i) an orbit *between* four antidots, denoted as (a), (ii) an orbit *around* one antidot (b), and (iii) orbit (c) emerging from a *bifurcation* of orbit (b). All other periodic orbits investigated play only minor roles: their $\partial S/\partial B$ is either too small (orbit bouncing between two antidots) or too large (longer periodic orbits). The $\tilde{S}(B)$ curves in Fig. 1(c) and Fig. 2 differ in their model parameters; we use $\beta = 2$ and $\hat{d} = 0.5$ for the solid, dashed, and dotted lines in Fig. 1(c) and $\beta = 4$ and $\hat{d} = 0.4$ for the traces in Fig. 2. Since $\hat{d}$ values are taken from the experiment [11] β is the only free parameter.

The calculated $\tilde{S}(B)$ traces in Fig. 1(c) and Fig. 2 closely follow the experiment and highlight the dominant role of the orbits (a), (b), and (c) [22]. The magnetic field dependence of $\tilde{S}(B)$ can be explained in a simplified approach evaluating the B dependence of the enclosed area $\mathcal{A}$. For unperturbed cyclotron motion $S(B) = eB\mathcal{A}$ holds, $\mathcal{A}(B) = \pi R_c^2$ scales with $1/B^2$, and $1/B$ periodic resistance oscillations result. At high B, orbit (a) is essentially unperturbed and in this realm oscillations periodic in $1/B$ are prominent in Figs. 1(c) and 2. At lower B where $2R_c$ is comparable to the period a, an essentially unperturbed cyclotron motion requires a sufficiently "open" antidot lattice (small $\hat{d}$, large β). $1/B$ periodic oscillations between $1/B = 1.3\ \mathrm{T}^{-1}$ and $2.5\ \mathrm{T}^{-1}$ in Fig. 2 document such behavior. Deviations from $\mathcal{A}(B) \propto 1/B^2$ destroy the $1/B$ periodicity: smaller action is caused by impeding the expansion of a cyclotron orbit. B periodic oscillations result when $\mathcal{A}$ is independent of B. This condition is closely fulfilled by orbit (b) calculated for $\beta = 2$, $\hat{d} = 0.5$ and shown in the bottom inset of Fig. 1(c). This trajectory encloses an area $\sim a^2$ causing the B periodic oscillations with $\Delta B \approx h/ea^2$ displayed in Fig. 1(b).

At low B, the system is nearly completely chaotic for $\beta = 2$ and $\hat{d} = 0.5$: the periodic orbits (a), (b), and (c) in Fig. 1(c) get unstable for B smaller than 0.6 T, 2.5 T, and 0.8 T, respectively. Why are the oscillations in ρ_{xx} determined by few periodic orbits with negligible volume in phase space? To obtain a picture of the classical phase space we trace classical trajectories, in general nonperiodic, starting normal to the Poincaré surface of section (boldface part of the diagonal in Fig. 3 inset). We integrate their normalized action $\mathcal{S}(B) = S(B)/eB\pi R_c^2$ until the electron traverses the diagonal for the second time. $\mathcal{S}(B)$ is visualized in a grey scale plot and shown as a function of $1/B$ and the electron starting position. Areas with rapidly changing $\mathcal{S}$ intersect regions with smoothly varying action. Solid lines in Fig. 3 mark the positions of the periodic orbits (a), (b), and (c) which minimize the action functional $\mathcal{S}$. The plot suggests that these orbits *represent the classical nonperiodic motion* in the extended regions of smoothly varying action. More specifically, by using the quantization condition Eq. (1) we implicitly performed a harmonic expansion of the action functional around the periodic orbits for nearby closed paths. Corresponding calculations show [23] that

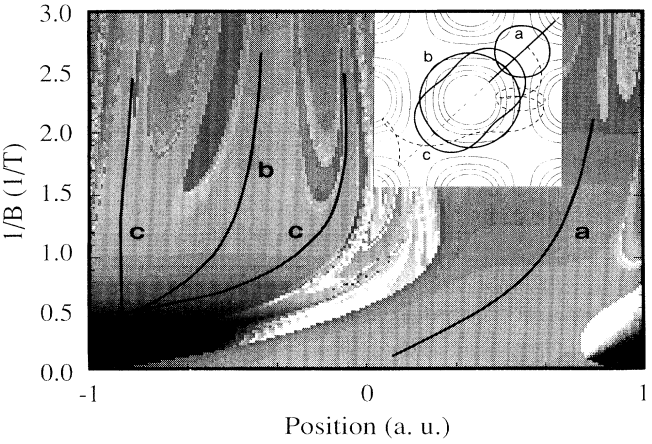

FIG. 3. Inset: Fundamental periodic orbits (a), (b), and (c) starting normal from the boldface segment of the diagonal. A nonperiodic, chaotic trajectory is shown as a dashed line. Parameters are $a = 200$ nm, $1/B = 0.74\ \mathrm{T}^{-1}$, $\hat{d} = 0.5$, and $\beta = 2$. The grey scale plot shows the normalized action for *all* trajectories starting from the diagonal segment as a function of $1/B$ and initial positions between -1 (lower left) and 1 (upper right). Maximum action: white. Minimum action: black. The initial conditions for the *periodic orbits* depicted in the inset are indicated by solid lines.

the harmonic approximation holds for large parts of the phase space around the orbits (a), (b), and (c) and hence explains their significance for the quantum oscillations reported here [24].

We thank B. Eckhardt, P. Fulde, T. Geisel, R. R. Gerhardts, R. Jalabert, A. Peck, D. Pfannkuche, U. Rau, and D. Wintgen for helpful discussions, and M. H. Pilkuhn for support. K.R. acknowledges financial support by the Humboldt Foundation. The work was sponsored by the Bundesministerium für Forschung und Technologie (TK 0366/5).

[a] On leave from Fakultät für Physik, Hermann-Herder-Strasse 3, 7800 Freiburg, Germany. Present address: Division de Physique Théorique, Institut de Physique Nucléaire, 91406 Orsay Cedex, France.

[1] For a review, see C. W. J. Beenakker and H. van Houten, in *Solid State Physics*, edited by H. Ehrenreich and D. Turnbull (Academic, New York, 1991), Vol. 44. p. 1, and references therein.

[2] For example, C. P. Umbach *et al.*, Phys. Rev. Lett. **56**, 386 (1986); K. Ismail, S. Washburn, and K. Y. Lee, Appl. Phys. Lett. **59**, 1998 (1991), and references therein. Note that the $h/2e$ periodic AB oscillations, not observed under the conditions of our experiment, only require ℓ_Φ to be of order a.

[3] M. L. Roukes and A. Scherer, Bull. Am. Phys. Soc. **34**, 633 (1989); K. Ensslin and P. M. Petroff, Phys. Rev. B **41**, 12 307 (1990).

[4] D. K. Ferry *et al.*, in *Electronic Properties of Multilayers and Low-Dimensional Semiconductor Structures*, edited by J. M. Chamberlain *et al.* (Plenum, New York, 1990); C. G. Smith *et al.*, J. Phys. Condens. Matter **2**, 3405 (1990); for a review, see D. K. Ferry, Prog. Quantum Electron **16**, 251 (1992).

[5] D. Weiss *et al.*, Phys. Rev. Lett. **66**, 2790 (1991).

[6] F. Nihey and K. Nakamura, Physica (Amsterdam) **184B**, 398 (1993).

[7] D. Weiss *et al.*, Appl. Phys. Lett. **58**, 2960 (1991).

[8] Under comparable experimental conditions $\ell_\Phi \sim 1 - 10\,\mu$m, see, e.g., T. Hiramoto, K. Hirakawa, Y. Iye, and T. Ikoma, Appl. Phys. Lett. **54**, 2103 (1989); A. Yacoby, U. Sivan, C. P. Umbach, and J. M. Hong, Phys. Rev. Lett. **66**, 1938 (1991).

[9] A. Lorke, J. P. Kotthaus, and K. Ploog, Phys. Rev. B **44**, 3447 (1991); T. Yamashiro *et al.*, Solid State Commun. **79**, 885 (1991).

[10] R. Fleischmann, T. Geisel, and R. Ketzmerick, Phys. Rev. Lett. **68**, 1367 (1992); R. Ketzmerick, R. Fleischmann, and T. Geisel (unpublished).

[11] Estimations of $\hat{d}$ are taken from Ref. [5].

[12] Spin splitting, resolved in the unpatterned segment, is not observed in the antidot array for $B < 3$ T ($\nu > 3$).

[13] T. Ando, A. B. Fowler, and F. Stern, Rev. Mod. Phys. **54**, 437 (1982); for modulated 2DEG's see D. Pfannkuche and R. R. Gerhardts, Phys. Rev. B **46**, 12 606 (1992).

[14] H. Silberbauer, J. Phys. C **4**, 7355 (1992).

[15] M. C. Gutzwiller, *Chaos in Classical and Quantum Mechanics* (Springer, New York, 1990); J. Math. Phys. **8**, 1979 (1967); **10**, 1004 (1969); **11**, 1791 (1970); **12**, 343 (1971).

[16] See M. V. Berry and K. T. Mount, Rep. Prog. Phys. **35**, 315 (1972), and references therein.

[17] For recent work see CHAOS **2** (1) (1992).

[18] Averaging of $d(E, B)$ over a finite intervall $\Delta E(\Delta B)$ is equivalent to the summation of trajectories up to finite times of motion $t < 2\pi\hbar/\Delta E$; see Ref. [24].

[19] W. H. Miller, J. Chem Phys. **63**, 996 (1975).

[20] D. Wintgen, K. Richter, and G. Tanner, CHAOS **2**, 19 (1992).

[21] Odd filling factors, not included in Eq. (4), label spin-split energy gaps.

[22] Deviations for $B < 0.4$ T in Fig. 2 are ascribed to orbits around *more* than one antidot. Those orbits are not considered here.

[23] K. Richter (unpublished).

[24] E. B. Bogomolny, Physica (Amsterdam) **31D**, 169 (1988).

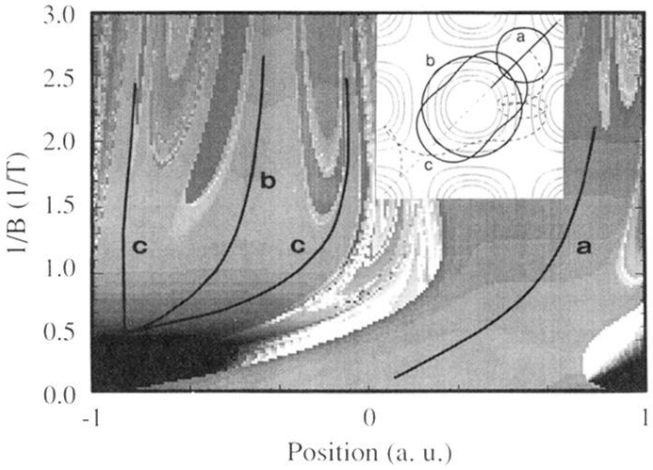

FIG. 3. Inset: Fundamental periodic orbits (a), (b), and (c) starting normal from the boldface segment of the diagonal. A nonperiodic, chaotic trajectory is shown as a dashed line. Parameters are $a = 200$ nm, $1/B = 0.74$ T^{-1}, $\hat{d} = 0.5$, and $\beta = 2$. The grey scale plot shows the normalized action for *all* trajectories starting from the diagonal segment as a function of $1/B$ and initial positions between -1 (lower left) and 1 (upper right). Maximum action: white. Minimum action: black. The initial conditions for the *periodic orbits* depicted in the inset are indicated by solid lines.